This article was downloaded by:
On: *25 January 2011*
Access details: *Access Details: Free Access*
Publisher *Taylor & Francis*
Informa Ltd Registered in England and Wales Registered Number: 1072954 Registered office: Mortimer House, 37-41 Mortimer Street, London W1T 3JH, UK


**Liquid Crystals**
Publication details, including instructions for authors and subscription information:
http://www.informaworld.com/smpp/title~content=t713926090

# Direct transition from the SmA phase to the tilted hexatic phase in liquid crystals with several lactate units

V. Novotná Corresponding author[a]; M. Kašpar[a]; V. Hamplová[a]; M. Glogarová[a]; I. Rychetský[a]; D. Pociecha[b]
[a] Institute of Physics, Academy of Sciences of the Czech Republic, 182 21 Prague 8, Czech Republic [b] Laboratory of Dielectrics and Magnetics, Chemistry Department, Warsaw University, 02-089 Warsaw, Poland

Online publication date: 12 May 2010

**To cite this Article** Novotná Corresponding author, V. , Kašpar, M. , Hamplová, V. , Glogarová, M. , Rychetský, I. and Pociecha, D.(2004) 'Direct transition from the SmA phase to the tilted hexatic phase in liquid crystals with several lactate units', Liquid Crystals, 31: 8, 1131 — 1141
**To link to this Article: DOI:** 10.1080/02678290410001720902
**URL:** http://dx.doi.org/10.1080/02678290410001720902

PLEASE SCROLL DOWN FOR ARTICLE

Full terms and conditions of use: http://www.informaworld.com/terms-and-conditions-of-access.pdf

This article may be used for research, teaching and private study purposes. Any substantial or systematic reproduction, re-distribution, re-selling, loan or sub-licensing, systematic supply or distribution in any form to anyone is expressly forbidden.

The publisher does not give any warranty express or implied or make any representation that the contents will be complete or accurate or up to date. The accuracy of any instructions, formulae and drug doses should be independently verified with primary sources. The publisher shall not be liable for any loss, actions, claims, proceedings, demand or costs or damages whatsoever or howsoever caused arising directly or indirectly in connection with or arising out of the use of this material.

LIQUID CRYSTALS, VOL. 31, NO. 8, AUGUST 2004, 1131–1141

Taylor & Francis
Taylor & Francis Group

# Direct transition from the SmA phase to the tilted hexatic phase in liquid crystals with several lactate units

V. NOVOTNÁ*, M. KAŠPAR, V. HAMPLOVÁ, M. GLOGAROVÁ, I. RYCHETSKÝ

Institute of Physics, Academy of Sciences of the Czech Republic, Na Slovance 2, 182 21 Prague 8, Czech Republic

and D. POCIECHA

Laboratory of Dielectrics and Magnetics, Chemistry Department, Warsaw University, Al. Zwirki i Wigury 101, 02-089 Warsaw, Poland

(*Received 28 November 2003; in final form 15 March 2004; accepted 26 March 2004*)

Compounds with differing numbers of lactate units in the chiral part were synthesized. For all materials, at least two smectic phases were found. In addition to the SmA, the SmC* and/or the tilted hexatic SmI*(F*) phase appear according to the length of the non-chiral alkyl chain. For the shortest non-chiral chain, a direct transition from the SmA phase to the SmI*(F*) phase has been discovered and studied. For compounds with the 2-(*S*)-methylbutyl alkyl chain and two lactate units in the chiral part the antiferroelectric $SmC_A^*$ phase occurs. The ferroelectric character of the hexatic phase has been confirmed even just below the $SmC_A^*$ phase.

Downloaded At: 16:48 25 January 2011

## 1. Introduction

New materials with two lactate units in the chiral part, and which exhibit a variety of chiral phases, have recently been synthesized [1]. All these materials, denoted **ZLL*m*/*n*** and **ZLL*m*/***, exhibited the SmA phase on cooling from the isotropic phase. Furthermore, for all these compounds, tilted hexatic phases were obtained on cooling from the ferroelectric (FE) SmC* phase or from the antiferroelectric (AF) $SmC_A^*$ phase. For the materials studied [1] the $SmC_A^*$ phase occurred only for compounds **ZLL*m*/*** with $m = 7$ or 8.

Here we describe the synthesis and properties of related liquid crystalline materials with different lengths of non-chiral alkyl chains and additional lactic acid units in the chiral part. The aim is to establish the effect of increasing the number of lactate units on the physical properties and the relationship between the non-chiral chain length and the phase sequence. The general molecular formulae used to refer to these materials are:

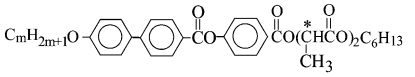

**ZLL *m*/6**

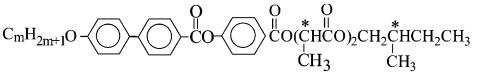

**ZLL *m*/***

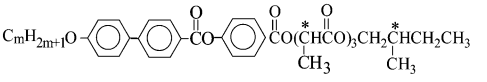

**ZLLL *m*/***

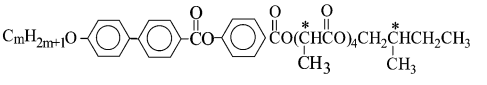

**ZLLLL *m*/***

The chiral chains contain two, three or four lactate groups and the designation of each compound includes the corresponding number of **L** letters. In addition, some homologues have an additional asymmetric centre in the 2-(*S*)-methylbutyl alkyl chain. The configuration of all chiral centers is *S*.

Materials **ZLL*m*/6** and **ZLL*m*/*** have been already studied [1] for $m = 6$, 7 and 8; they exhibit the SmA–$SmC^*$–$SmC_A^*$–SmI*(F*) or SmA–SmC*–SmI*(F*) phase sequences. The ferroelectric character of the tilted hexatic phase has already been established [2]. In compound **ZLL7/*** the ferroelectric re-entrant SmC* phase below the $SmC_A^*$ phase was detected. With all compounds studied in [1], a significant decrease of both the spontaneous tilt, $\theta_S(T)$, and spontaneous

*Author for correspondence; e-mail: novotna@fzu.cz

*Liquid Crystals* ISSN 0267-8292 print/ISSN 1366-5855 online © 2004 Taylor & Francis Ltd
http://www.tandf.co.uk/journals
DOI: 10.1080/02678290410001720902

polarization, $\mathbf{P}_S(T)$, was observed when entering the hexatic phase from the SmC* or $SmC^*_A$ phases.

In all the materials described here, at least two smectic phases have been observed and the phase transition to the hexatic phase has been studied. In addition, the direct phase transition from the SmA to the tilted hexatic phase is reported for the first time in this contribution.

## 2. Synthesis

The synthetic route is outlined in the scheme. The synthesis of compounds **ZLL*m*/6** and **ZLL*m*/*** with two

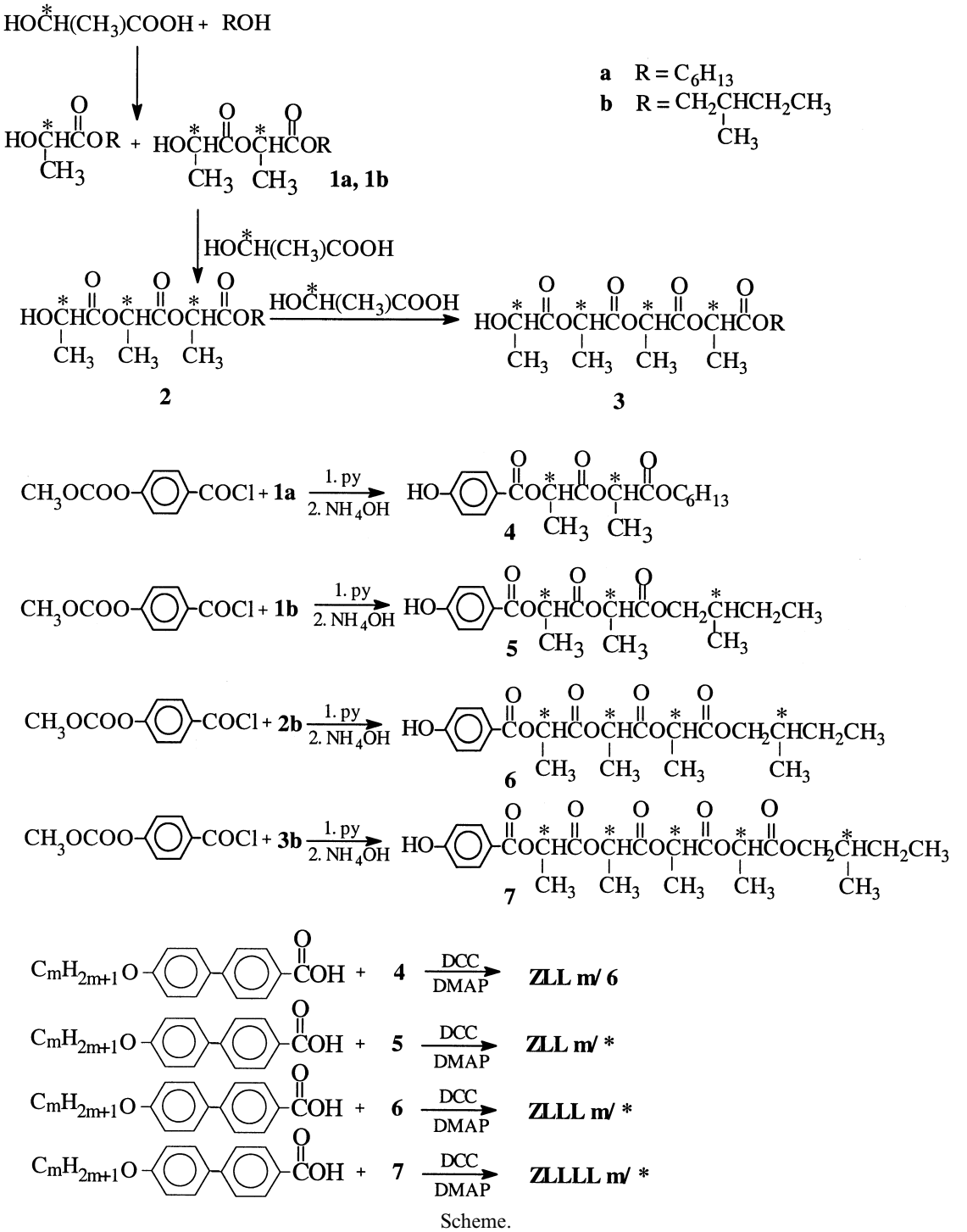


Scheme.

Downloaded At: 16:48 25 January 2011

lactate groups in the chiral chain has been described recently in detail elsewhere [1].

### 2.1. *Synthesis of compounds* **ZLLL*m*/*** *and* **ZLLLL*m*/***

A 30 g portion the required of α-(*S*)-(alkyloxycarbonyl) ethyl-(*S*)-lactate (**1a** or **1b**) and 50 g of L-lactic acid were heated under reflux in a Dean–Stark trap with benzene for 24 h. The mixture was cooled and washed twice with water to remove excess lactic acid. The solution was dried with sodium sulphate and filtered. Benzene was evaporated off and the remainder was destilled in vacuum: the first fraction (b.p. 100–120°C/1 torr) was unreacted lactate dimer (**1a**, **1b**) and lactide; the second fraction was lactate trimer **2** (b.p. 135°C/1 torr for compound **2b**). Lactate trimer **2** contained a small amount of lactate tetramer **3**, which was impossible to separate by distillation. They were reacted together to compounds **6** and **7** and then with 4-alkoxybiphenyl-4′-carboxylic acid to give the mixture of final compounds **ZLLL*m*/*** and **ZLLLL*m*/*** by the procedure described in [1]. The separation of these two very similar compounds was carried out by high pressure liquid chromatography on a preparative scale on a modular isocratic chromatograph Ecom. A preparative column (Watrex, 400 × 32 mm) with Biospher SI 100–12 μm, equipped with a guard column (Watrex 100 × 25 mm) with the same sorbent, was used. A mixture of 99.8% of toluene and 0.2% of methanol was used as eluant. Detection of the eluting products was carried out by a UV-Vis detector ($\lambda = 290$ nm). Fractions, 5 ml each, of eluting solution were collected, analysed and these selected that contained **ZLLL*m*/*** and **ZLLLL*m*/*** in purity above 99.8%.

Downloaded At: 16:48 25 January 2011

### 2.2. *NMR spectra*

The structures of all intermediates and final products were confirmed by $^1$H NMR (200 MHz, $CDCl_3$, Varian, Gemini 2000).

**1a**: 5.17 q, $J = 7.0$, (1H, –COOC*HCOO–); 4.35 q, $J = 7.0$, (1H, HOC*H); 4.13 t + t, $J_1 = 6.6$, $J_2 = 1.1$, (2H, $COOCH_2$); 1.63 quint, $J = 6.6$ (2H, $COOCH_2\underline{CH_2}$); 1.20–1.35 m (6H, $CH_2$); 1.52 and 1.48 d + d, $J = 7.0$ (3 + 3H, $\underline{CH_3}$–C*H); 0.88 t, $J = 6.5$ (3H,$CH_3$).

**1b**: 5.15 q, $J = 7.0$ (1H, –COOC*HCOO–); 4.30 q, $J = 7.0$ (1H, HO$\underline{C*H}$); 3.95 m (2H, $COOCH_2$); 1.70 m (1H, $\underline{C*H}CH_2$); 1.4–1.5 dd, $J = 7$ (3 + 3H, $\underline{CH_3}C*H$); 1.35 and 1.15, m + m (2H, $C*HCH_2$); 0.88 m (6H, $CH_3$).

**2b** ($R = CH_2CH(CH_3)CH_2CH_3$): 5.1–5.2 m (2H, COOC*HCOO); 4.30 q, $J = 7.0$ (1H, HO$\underline{C*H}$); 3.95 m (2H, $COOCH_2$); 1.70 m (1H, $\underline{C*H}CH_2$); 1.60 and 1.50 and 1.45 d + d + d, $J = 7$ (9H, $\underline{CH_3}C*H$); 1.35 and 1.15 m + m (2H, $C*H\underline{CH_2}$); 0.88 m (6H, $CH_3$).

**4**: 7.90 d, $J = 8.8$ (2H, ArH *ortho* to –COO); 6.80 d, $J = 8.8$ (2H, ArH *ortho* to OH); 5.30 q, $J = 7.1$ (1H, ArCOO$\underline{C*H}$); 5.15 q, $J = 7.0$, (1H, C*H); 4.10 m (2H, $COOCH_2$); 1.65 and 1.50 d + d, $J = 7.0$ (6H, $\underline{CH_3}C*H$); 1.2–1.7 m (6H, $CH_2$); 0.9 t, $J = 6.6$ (3H, $CH_3$).

**5**: 7.90 d, $J = 8.8$ (2H, ArH *ortho* to –COO); 6.80 d, $J = 8.8$ (2H, ArH *ortho* to –OH); 5.35 q, $J = 7.0$ (1H, ArCOO$\underline{C*H}$); 5.20 q, $J = 7.0$ (1H, COO$\underline{C*H}$COO); 4.00 m (2H, COO$\underline{CH_2}$); 1.65 and 1.55 d + d, $J = 7.0$ (6H, $CH_3C*H$); 1.60 m (1H, $\underline{C*H}CH_2$); 1.4 and 1.2, m + m (2H, $C*H\underline{CH_2}$); 0.90 m (6H, $CH_3$).

**6**: 7.90 d, $J = 8.8$ (2H, ArH *ortho* to –COO); 6.80 d, $J = 8.85$ (2H, ArH *ortho* to –OH); 5.40 q, $J = 7.1$ (1H, ArCOOC*H); 5.20 m (1 + 1 H, COO$\underline{C*H}$COO); 4.02 m (2H, $COOCH_2$); 1.70 and 1.62 and 1.52, d + d + d, $J = 7$ (9H, $\underline{CH_3}C*H$); 1.60 m (1H, $\underline{C*H}CH_2$); 1.4 and 1.2, m + m (2H, $C*H\underline{CH_2}$); 0.92 m (6H, $CH_3$).

**ZLLL 9/***: 8.20 dd, (4H, ArH *ortho* to –COO); 7.6–7.7 m, $J = 8.6$ (4H, ArH *ortho* to –Ar); 7.33 d, $J = 8.6$, (2H, ArH *ortho* to –OCOAr); 7.00 d, $J = 8.8$ (2H, ArH *ortho* to –O*R*); 5.40 q, $J = 7.1$ (1H, ArCOOC*H); 5.20 m (1 + 1H, COO$\underline{C*H}$COO); 4.02 m (4H, $\underline{CH_2}$OAr and COO$\underline{CH_2}$); 1.72 and 1.62 and 1.52, d + d + d (9H, $\underline{CH_3}C*H$); 1.3–1.9 m (17 H, $CH_2$, C*H); 0.92 m (9H, $CH_3$).

**ZLLLL 9/***: 8.20 dd, (4H, ArH *ortho* to –COO); 7.6–7.7 dd, $J = 8.6$ (4H, ArH *ortho* to –Ar); 7.33 d, $J = 8.6$, (2H, ArH *ortho* to –OCOAr); 7.00 d, $J = 8.8$ (2H, ArH *ortho* to –O*R*); 5.40 q, $J = 7.1$ (1H, ArCOOC*H); 5.20 m (3H, COO$\underline{C*H}$COO); 4.02 m (4H, $\underline{CH_2}$OAr and COO$\underline{CH_2}$); 1.72 and 1.62 and 1.57 and 1.52, 4 × d (12H, $\underline{CH_3}C*$); 1.3–1.9 m (17 H, $CH_2$, C*H); 0.92 m (9H, $CH_3$).

## 3. Experimental

### 3.1. *Characterization*

The liquid crystalline phases were firstly identified by the observation of optical textures. The polarizing microscope Nikon Eclipse E-600 was used and studies were carried out on samples in a book-shelf (planar) geometry, the sample thickness was 6, 25 or 50 μm. The cells, consisting of glass plates coated with ITO electrodes and polyimide layers unidirectionally rubbed, were filled in the isotropic phase. Phase transitions were studied by DSC measurements (Perkin-Elmer Pyris Diamond). Samples of about 3 mg were hermetically closed in aluminium pans; heating and cooling rates of 5 K min$^{-1}$ were used.

The spontaneous polarization $\mathbf{P}_s$ was measured using a Sawyer–Toyer bridge and determined from **P**(**E**) hysteresis loops taken at a frequency of 50 Hz. The

temperature was varied and stabilized with an accuracy of $\pm 0.1^{\circ}$C in the hot stage (Linkam). The spontaneous tilt angle $\theta_s$ was determined from the angle difference between minimum transmission (extinction) positions under crossed polarizers, measured under opposing d.c. electric fields (about $40\,\mathrm{kV\,cm^{-1}}$).

The helicoidal pitch $p$ was established from the diffraction of He-Ne laser light on dechiralization lines, which exist in planar samples due to strong polar anchoring at the surfaces. This method is applicable when the value of $p$ lies within the interval approximately $0.8\,\mu\mathrm{m} < p < 8\,\mu\mathrm{m}$. For measurements of pitch, thick planar samples (50 μm) were used. Free-standing films of several hundreds μm thick were prepared by spreading the material over a 1-mm diameter hole in a metal plate and observed under the polarizing microscope.

X-ray studies were performed using a DRON system equipped with a Ge monochromator. Experiments were conducted on non-oriented samples in the reflection mode.

Dielectric properties were studied using a Schlumberger 1260 impedance analyser. The frequency dispersions were measured on cooling at a rate of about $0.2\,\mathrm{K\,min^{-1}}$, keeping the temperature of the sample stable during frequency sweeps in the range 10 Hz–1 MHz. The frequency dispersion data were analysed using the Cole–Cole formula for the frequency-dependent complex permittivity $\varepsilon^*(f) = \varepsilon' - \mathrm{i}\varepsilon''$:

$$\varepsilon^* - \varepsilon_\infty = \frac{\Delta\varepsilon}{1 + (if/f_r)^{(1-\alpha)}} - \mathrm{i}\frac{\sigma}{2\pi\varepsilon_0 f^n} + Af^m \qquad (1)$$

where $f_r$ is the relaxation frequency, $\Delta\varepsilon$ is the dielectric strength, $\alpha$ is the distribution parameter of the relaxation, $\varepsilon_0$ is the permittivity of a vacuum, $\varepsilon_\infty$ is the high frequency permittivity and $n$, $m$, $A$ are fitting parameters. The second and third terms in the equation are used to eliminate a low frequency contribution from d.c. conductivity $\sigma$ and a high frequency contribution due to resistance of the ITO electrodes, respectively.

### 3.2. *Mesomorphic properties*

The phase transition temperatures and enthalpies were evaluated from DSC studies (see the table). Typical DSC plots are shown in figures 1 (*a–c*). In figure 1 (*c*) for compound **ZLL9/***, a negative peak is seen in DSC plots taken on heating which corresponds to a partial recrystallization. This anomaly persists even on cooling the compound to $\approx -40^{\circ}$C before subsequent heating. We also note the transition peaks to the hexatic phase which possess characteristic broad wings on both sides, a consequence of pre-transitional thermal fluctuations [3].

Phases were identified from observations of their textures and how these change. All materials studied exhibit the SmA phase on cooling from the isotropic

Table 1. Melting points (m.p.), phase transition temperatures phases and associated transition enthalpies (in square brackets). Symbols: • the phase exists,—the phase does not exist. $T_c$, $T_A$ and $T_{hex}$ are the transition temperatures of the SmA–SmC*, SmC*–SmC$^*_A$ and SmC* (SmC$^*_A$)–SmI*(F*) phase transitions, respectively.

| Compound | m.p./°C [$\Delta H$/J g$^{-1}$] | $T_{tr}$/°C [$\Delta H$/J g$^{-1}$] | SmX | $T_{tr}$/°C [$\Delta H$/J g$^{-1}$] | hex. | $T_{hex}$/°C [$\Delta H$/J g$^{-1}$] | SmC$_A$* | $T_A$/°C [$\Delta H$/J g$^{-1}$] | SmC* | $T_c$/°C [$\Delta H$/J g$^{-1}$] | SmA | $T_{tr}$/°C [$\Delta H$/J g$^{-1}$] | I |
|---|---|---|---|---|---|---|---|---|---|---|---|---|---|
| **ZLL 5/6** | 75 [4.4] | 42 [−0.3] | • | 73 [−4.3] | • | 80 [−2.8] | — | | — | — | • | 143 [−7.4] | • |
| **ZLL 9/6** | 79 [52.5] | 39 [−16.5] | — | | • | 42 [−0.3] | — | | • | 94 [−0.35] | • | 113 [−2.7] | • |
| **ZLL 5/*** | 80 [24.5] | 30 [−3.5] | • | 79 [−4.4] | • | 87 [−3.4] | — | | — | | • | 146 [−9.2] | • |
| **ZLL 9/*** | 83 [17.1] | 37 [−14.6] | — | | • | 43 [−0.9] | • | 99 [−0.1] | • | 105 [−0.54] | • | 118 [−3.3] | • |
| **ZLLL 5/*** | 80 [24.5] | 56 [−1.4] | • | 76 [−3.5] | • | 85 [−3.4] | — | | — | | • | 136 [−9.2] | • |
| **ZLLL 7/*** | 67.5 [25.6] | 60 [−11.7] | — | | • | 72 [−2.2] | — | | • | 104 [−0.5] | • | 128 [−12.7] | • |
| **ZLLL 8/*** | 68 [28.6] | 56 [−11.9] | — | | • | 62 [−0.7] | — | | • | 96 [−0.2] | • | 120 [−9.9] | • |
| **ZLLL 9/*** | 88 [36.6] | 51 [−19.1] | — | | • | 60 [−1.1] | — | | • | 100 [−0.5] | • | 117 [−3.2] | • |
| **ZLLLL 5/*** | 71 [13.6] | 55 [−1.26] | • | 68 [−2.8] | • | 78 [−2.4] | — | | • | 86 [−0.55] | • | 120 [−5.3] | • |
| **ZLLLL 9/*** | 70 [11.9] | 49 [−13.9] | — | | — | | — | | • | 88 [−0.2] | • | 98 [−0.4] | • |

Downloaded At: 16:48 25 January 2011

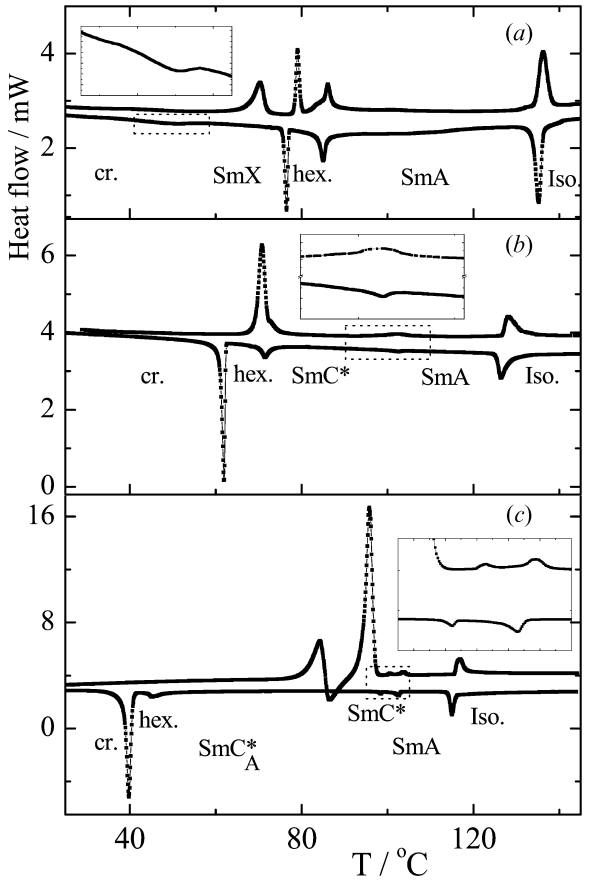


Figure 1. Typical DSC plots for compounds (*a*) **ZLLL5/***, (*b*) **ZLLL7/*** and (*c*) **ZLL9/***. The upper and lower curves show second heating and cooling runs, respectively. The dotted rectangles indicate weak phase transitions, which are seen enlarged in the insets. The slopes are adjusted for convenience, phases are indicated.

phase. At lower temperatures, the SmC* phase appears, except for materials with the shortest non-chiral chain **ZLL5/***, **ZLL5/6** and **ZLLL5/***, for which the SmI*(F*) phase appears just below the SmA phase. The antiferroelectric smectic $SmC^*_A$ phase exists only in the **ZLL*m*/*** series for $m=7$, 8, 9. The antiferroelectric character of the $SmC^*_A$ phase and the ferroelectricity nature of the hexatic phase were confirmed by dielectric and switching studies (see later).

The phase diagrams for the homologous series **ZLL*m*/6**, **ZLL*m*/*** and **ZLLL*m*/*** are shown in figures 2 (*a*, *b*, *c*), respectively. In figures 2 (*a*) (**ZLL*m*/6**) and 2 (*b*) (**ZLL*m*/***) the phase transition temperatures already published [1] for $m=6$, 7 and 8 are also included.

### 3.3. *Spontaneous quantities and switching properties*

The temperature dependence of the spontaneous polarization $\mathbf{P}_S$ and spontaneous tilt angle, $\theta_S$, exhibit typical increases on cooling in the SmC* phase, see figure 3 (*a*) for **ZLLL7/***. In **ZLL9/*** the $SmC^*_A$ phase was found. Antiferroelectricity was confirmed from switching properties using a triangular wave field of $20\,V\,\mu m^{-1}$ and a frequency below 20 Hz. Specifically, two distinct peaks in the polarization reversal current characteristic for antiferroelectric switching are clearly seen. The threshold field in the antiferroelectric phase (about $5\,V\,\mu m^{-1}$) is much larger then in the SmI*(F*) phase, for which only one peak in the polarization reversal current was detected. We conclude that the hexatic phase is ferroelectric. At the SmC*–$SmC^*_A$ phase transition no anomalies in $\mathbf{P}_S$, or $\theta_S$, occur. The

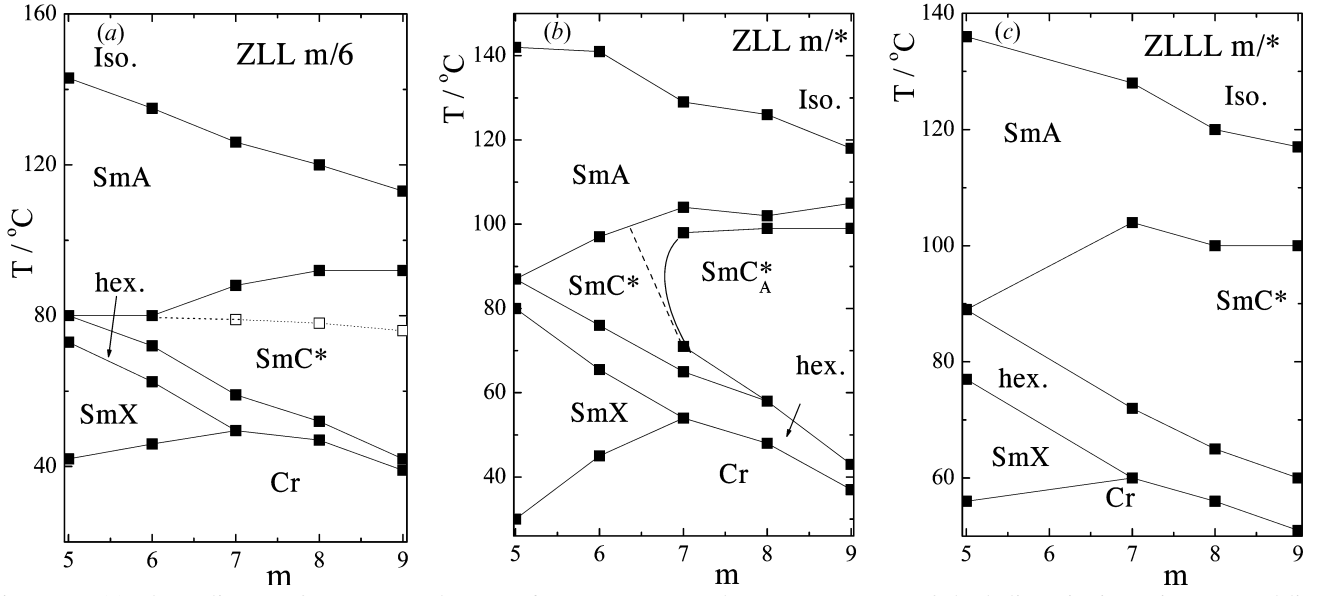


Figure 2. (*a*) Phase diagram for compounds **ZLL*m*/6**. Open squares show temperatures of the helix twist inversion. Dotted line separates regions of different helicity sign; (*b*) phase diagram for compounds **ZLL*m*/***; (*c*) phase diagram for compounds **ZLLL*m*/***.

Downloaded At: 16:48 25 January 2011

same result was found for **ZLL7/*** and **ZLL8/*** [1].

Significant decreases of $\theta_S(T)$ and $\mathbf{P}_S(T)$ were observed when entering the hexatic phase from the SmC* phase or from the $SmC^*_A$ phase, see figure 3 (*a*) for **ZLLL7/***. This decrease may be explained theoretically by the change of the pitch caused by the increase of bond orientation order [4]. For homologues with $m=5$, where the hexatic phase is reached directly from the SmA phase, both $\mathbf{P}_S$ and $\theta_S$ start to grow on cooling from the first order SmA–SmI(F)* phase transition to a maximum, see figure 3 (*b*) for **ZLL5/***. The subsequent decrease of $\mathbf{P}_S$ and $\theta_S$ values when approaching the phase transition to the crystal-like SmX phase may be connected with incomplete switching due to the increase of viscosity.

### 3.4. *X-ray measurements*

The temperature dependence of the layer spacing $d(T)$ is shown in figures 4 (*a*) and 4 (*b*) for compounds **ZLLL9/*** and **ZLL5/***, respectively. In the SmA phase a typical increase of $d$ is seen on cooling. At the SmA–SmC* phase transition $d$ clearly shows a characteristic decrease at the onset of the tilted SmC* phase on cooling, which reflects the molecular tilt. On subsequent

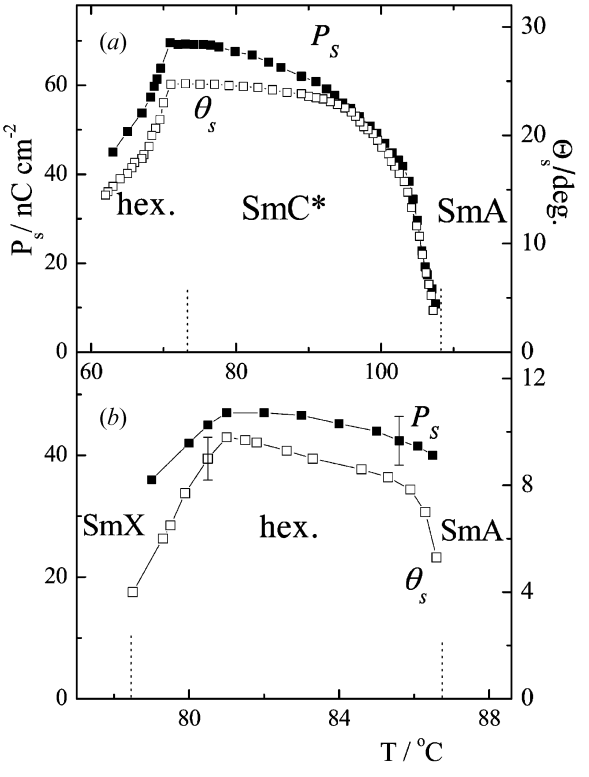


Figure 3. Temperature dependence of the spontaneous polarization $\mathbf{P}_S$ and spontaneous tilt angle $\theta_S$, for compounds (*a*) **ZLLL7/*** and (*b*) **ZLL5/***.

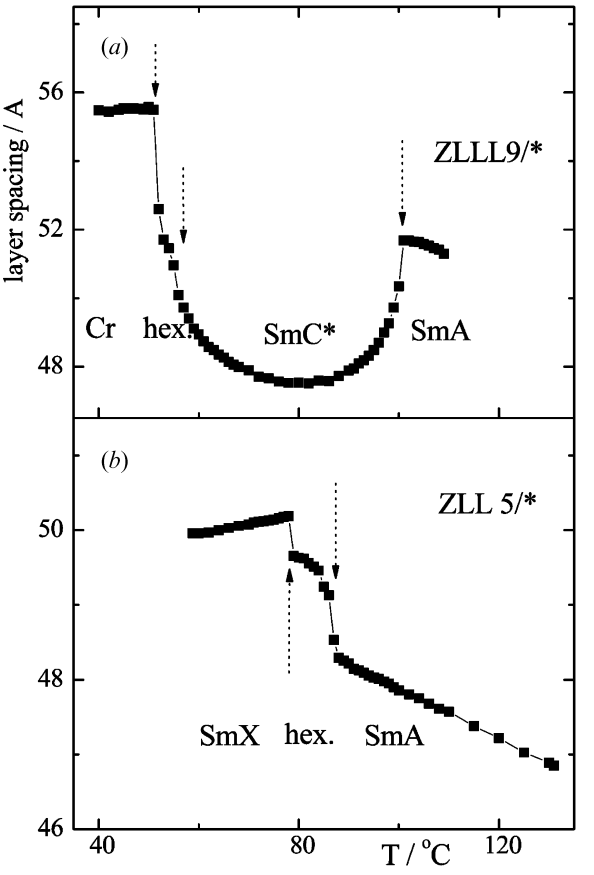


Figure 4. Temperature dependence of the layer spacing for compounds (*a*) **ZLLL9/*** and (*b*) **ZLL5/***.

cooling, $d$ starts to increase within the SmC* phase and the inflection point in the increase represents the phase transition to the hexatic phase, see figure 4 (*a*). The increase of $d$ in the SmC* phase is caused by pretransitional effects before the transition to the hexatic phase [5], in which $d$ increases due to the stretching of aliphatic molecular chains and the increase of orientational order of the long molecular axes [6, 7]. In the hexatic phase $d$ might be even higher than in the non-tilted SmA phase. In homologues with the direct SmA–SmI*(F*) phase transition a step increase of $d$ values is associated with the phase transition to the hexatic phase, figure 4 (*b*), which seems to be a little surprising, because it is a transition from an orthogonal to a tilted phase. A higher $d$ value in the hexatic phase means that the tilt is compensated by the increase of the orientational order parameter and the stretching of terminal chains. On further cooling, the $d(T)$ dependence exhibits an additional pronounced step increase at the phase transition to the low temperature SmX phase see figures 4 (*a*) and 4 (*b*).

Downloaded At: 16:48 25 January 2011

### 3.5. *Helical properties*

In the planar geometry, the dechiralization lines appear just below the transition temperature ($T_c$) to the SmC* phase, and are a consequence of the existence of the helical structure. The temperature dependence of the helical pitch $p$ was established by the diffraction of laser light on the dechiralization lines. For **ZLL*m*/6**, $m = 7,8$ and 9, the pitch shows a remarkable increase on cooling, and at some temperature range $p$ cannot be measured as the diffraction pattern disappears, which is connected with the disappearance of dechiralization lines and a complete unwinding the helical structure. On subsequent cooling the lines start to reappear spontaneously or can be generated by a small electric field, the helical pitch steeply decreasing, figure 5 (*a*). The spontaneous helix unwinding should be connected with a twist inversion. To confirm this, we studied the rotatory power of free-standing films. In figure 5 (*a*) we compare the temperature dependence of the pitch measured on a planar sample (50 μm) with the rotatory power obtained on thick free-standing film (about 100 μm) for compound **ZLL8/6**. One can see a continuous change of the rotatory power with temperature and a step-like change of its sign in the temperature range in which the helix is unwound. The change of sign corresponds to the inversion of the helix twist. We defined the helix twist inversion temperature $T_i$ as the centre of the region, about 8 K wide, in which no optical rotation and also no helix were detected. In the phase diagram in figure 2 (*a*) the temperatures of the helix twist inversion for homologues **ZLL7/6**, **ZLL8/6**, and **ZLL9/6** are denoted by open squares.

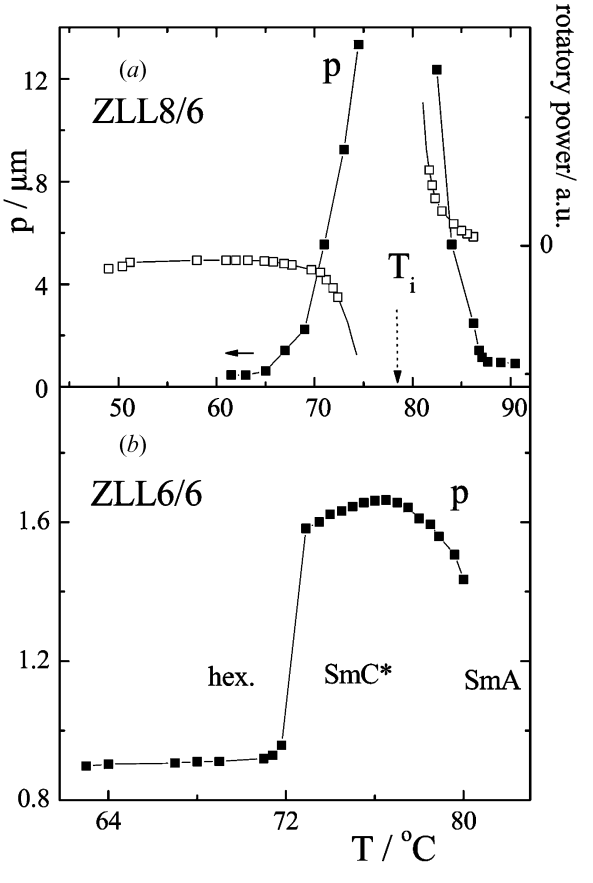


Figure 5. Temperature dependence of the pitch length (full symbols) measured on a 100 μm thick planar sample for compound (*a*) **ZLL8/6** and (*b*) **ZLL6/6**. On the right hand side of (*a*) the temperature dependence of rotatory power is shown for **ZLL8/6** (open symbols).

Within the temperature interval of the helix unwinding, a striped or rectangular texture is observed in thick free-standing films (see figure 6). Such a texture has already been described for another material exhibiting a helix twist inversion [8]. A spontaneous in-plane director modulation is the origin of this texture.

In **ZLL6/6** dechiralization lines exist over the whole temperature range of both ferroelectric phases. The temperature dependence of the pitch length reveals a discontinuous decrease at the SmC*–SmI*(F*) phase transition, see figure 5 (*b*). To distinguish the sign of helicity of **ZLL6/6** and **ZLL7/6** we prepared a contact sample in the planar geometry. In the contact area of **ZLL6/6** and **ZLL7/6** dechiralization lines were observed in the whole temperature range of the SmC* phase of **ZLL6/6**, showing the same sign of helicity in both compounds. Based on this finding we drew the dotted line in figure 2 (*a*), which separates the regions with opposite helix handedness for the homologous series **ZLL*m*/6**.

In homologue **ZLL7/*** the helix twist inversion takes place at the phase transition to the reentrant SmC* phase [2]. Here we prepared contact samples and found that at the contact area between compounds **ZLL7/*** and **ZLL6/*** no dechiralization lines occur, which demonstrates the unwound structure due to the opposite helicity of the two compounds. Two additional contact samples for each of compounds **ZLL6/*** and **ZLL7/*** with a chemically similar material K8/4 were studied. Compound K8/4 exhibits a wide temperature range SmC* phase with a practically constant pitch length of about 1.5 μm [9]. We found that the helicity sign in the SmC* and $SmC^*_A$ phases of **ZLL7/***, **ZLL8/*** and **ZLL9/*** is opposite to that in the SmC* phase of **ZLL6/***. In the phase diagram of homologues **ZLL*m*/***, figure 2 (*b*), we can draw the dotted line, which separates opposite helicity areas.

For the series **ZLLL*m*/*** with $m = 7$, 8 and 9, the helix unwinds when approaching the SmC*–SmI*(F*) phase transition on cooling and remains unwound in the hexatic phase. In the temperature range of the helix unwinding, the dechiralization lines disappear in planar

Downloaded At: 16:48 25 January 2011

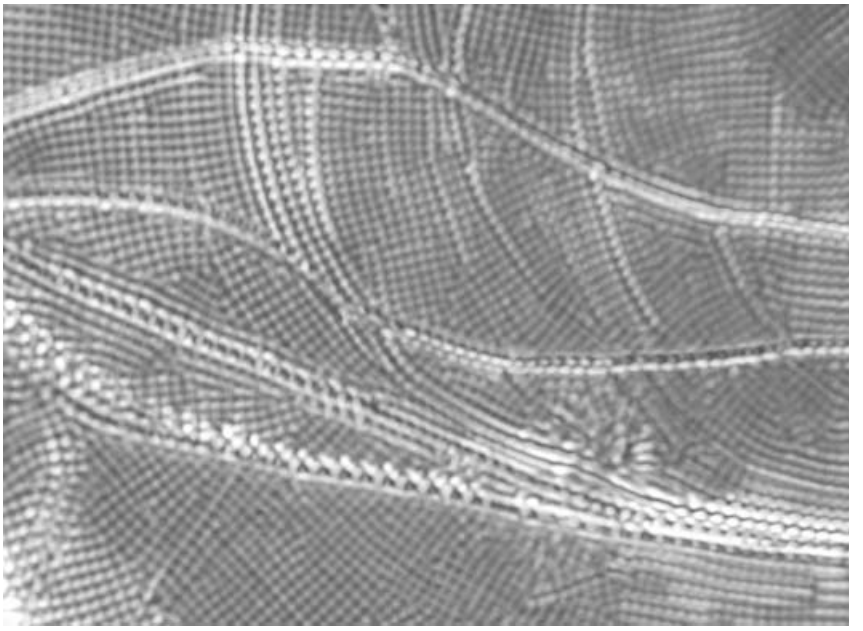

Figure 6. Texture of free-standing film taken at 74°C for the compound **ZLLL9/***. The width of the photomicrograph is about 100 μm.

Downloaded At: 16:48 25 January 2011

samples and the texture reflecting the in-plane modulation is seen in the free-standing films; see figure 6 for compound **ZLLL9/***.

### 3.6. *Dielectric spectroscopy*

For compounds with a short alkyl chain, e.g. $m=5$, the hexatic phase is obtained directly from the SmA phase on cooling. The frequency dependence of the complex permittivity, $\varepsilon^*(f)$, shows a single relaxation process in both phases (see figure 7). Fitted values of the relaxation frequency $f_r$ and dielectric strength $\Delta\varepsilon$ are shown in figure 8 (*a*) for **ZLL5/***. A typical feature is a broad maximum in $\Delta\varepsilon$ around the SmA–SmI*(F*) phase transition and a continuous decrease of $f_r$ on cooling.

For materials with the SmC* phase, the dielectric spectra show a strong soft mode (fluctuation of the molecular tilt) in the paraelectric SmA phase. Its relaxation frequency $f_r$ decreases almost linearly, as shown in figure 8 (*b*) for **ZLL7/***; dielectric strength $\Delta\varepsilon$ steeply increases when approaching the SmA–SmC* phase transition on cooling, the maximum in $\Delta\varepsilon$ indicating the phase transition. The Goldstone mode (fluctuation of the azimuthal molecular orientation) in the SmC* phase exhibits low $f_r$ and high $\Delta\varepsilon$, both being only slightly temperature dependent, see figure 8 (*b*). If the compound exhibits the helix unwinding in the SmC* phase, a step down in $f_r(T)$ and increase in $\Delta\varepsilon(T)$ occur below $T_i$ on cooling; see figure 8 (*c*) for **ZLL8/6**. Anomalies in the vicinity of $T_i$ for the temperature dependences of $f_r(T)$ and $\Delta\varepsilon(T)$ have been observed in a different type of materials exhibiting a helix twist inversion [10].

In the antiferroelectric $SmC_A^*$ phase a high frequency mode occurs. Just below the upper SmC* phase this mode is barely detectable because of its very high relaxation frequency, which decreases on cooling. At lower temperatures the relaxation is detected, but $\Delta\varepsilon$ is very low; see figure 8 (*d*) for **ZLL9/***. This mode can be interpreted as the antiphase azimuthal motions of molecules in neighbouring layers or as a mode due to distortion of the whole helix (in-phase azimuthal motions of molecules in neighbouring layers, the Goldstone mode). The latter mode should possess lower frequency and is dielectrically active due to the non-compensated polarization in the helical smectic layer structure. Such a mode was reported in [11], where it was suggested that it was responsible for the increase of permittivity near the ferrielectric–AF phase transition. A theoretical description of such a mode may be found in [12].

For **ZLL9/*** and **ZLL8/***, where the SmI*(F*) phase lies just below the $SmC_A^*$ phase, the dielectric mode with a relatively high dielectric strength ($\Delta\varepsilon\sim40-100$) and low relaxation frequency ($f_r\sim50$–$200$ Hz) has been detected in the hexatic phase, see figure 9. It is consistent with ferroelectric character of the observed hexatic phase.

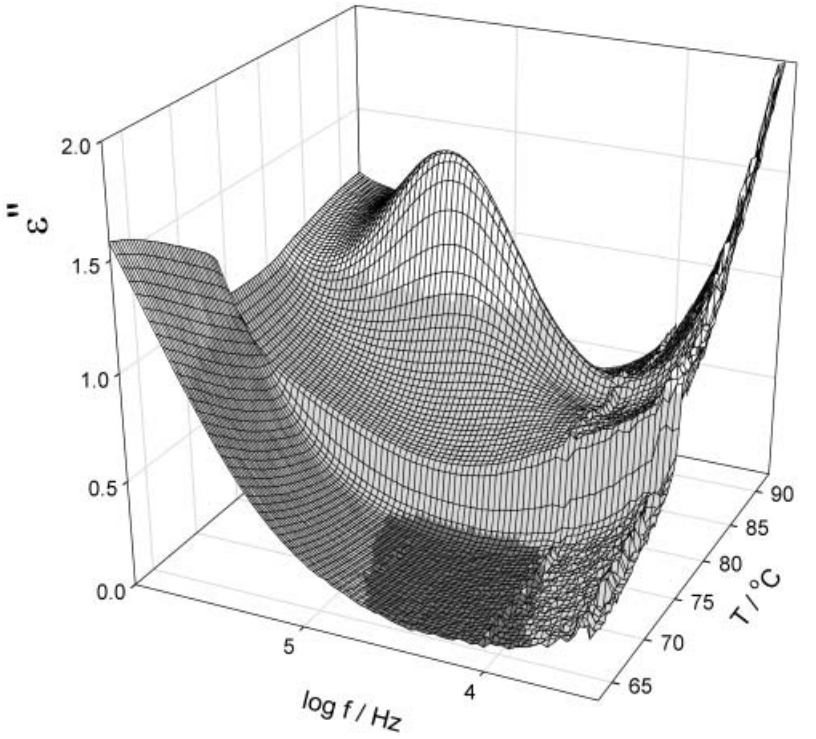


Figure 7. Temperature–frequency plots of the imaginary dielectric permittivity taken on cooling from the SmA to the hexatic phase for compound **ZLL5/***.

Downloaded At: 16:48 25 January 2011

## 4. Discussion and conclusions

All the materials studied exhibit the SmA phase and the ferroelectric tilted hexatic SmI* (or SmF*) phase, except for **ZLLLL 9/*** for which the hexatic phase is missing. The SmC* phase does not exist for compounds with a short non-chiral chain ($m=5$). In these compounds the direct SmA–SmI*(F*) transition is observed. This phase transition has not been reported to data. According to theory [12] such a phase transition can occur when $T_C \approx T_{hex}$, and it should be discontinuous in both the bond orientation order $A$ and the tilt. In accord with the theory, jumps of $\mathbf{P}_s$ and $\theta_s$ have been observed at the SmA–hexatic phase transition (a first order phase transition). In the case of a sufficiently small tilt at the transition region, theory predicts a more complicated double-modulated structure (incommensurate in $A$ and $\theta$ modulations) [4, 12], but is expected to be undetectable in dielectric spectra.

No anomaly was found in the temperature dependences of the spontaneous polarization and spontaneous tilt angle at the SmC*–SmC$^*_A$ phase transition. Both spontaneous quantities, $\mathbf{P}_s$ and $\theta_s$, decrease when entering the SmI*(F*) phase from the SmC* or SmC$^*_A$ phases on cooling. In [4] the decrease $\Delta\theta_S$ of the spontaneous tilt is explained as the result of the change of the pitch caused by the increasing hexatic order. It was shown that $\Delta\theta_S \propto (q-q_\theta)^2$, where $q_\theta$ and $q$ are vectors of modulation that correspond to SmC* and the hexatic phases, respectively, the latter depending on the bond orientation order.

The increase in layer spacing on cooling within the temperature range of the SmA phase is caused by an increase in the effective molecular length (the projection of the molecule on the layer normal), which may occur due to the increase of molecular orientation order (nematic order parameter). The layer spacing decreases below the SmA–SmC* phase transition because of the increasing molecular tilt. When entering the tilted hexatic phase (even if it is reached directly from the SmA phase) the layer spacing increases due to increased molecular order and probably due to an extension of terminal chains. These mechanisms can also influence the strengths of interactions of molecular tilts, and interactions between the tilt and the bond order. It would cause the temperature dependence of the free energy coefficients (i.e. also their change at the hexatic transition), which were considered constant in [4]. Such a temperature behaviour could be another reason for the tilt angle decrease in the hexatic phase.

Dielectric spectroscopy confirmed a strong soft mode in the SmA phase above both the SmA–SmC* and SmA–SmI*(F*) transitions. In the SmC* phase the Goldstone mode is the main contribution to the dielectric response. The dielectric strength $\Delta\varepsilon$ of

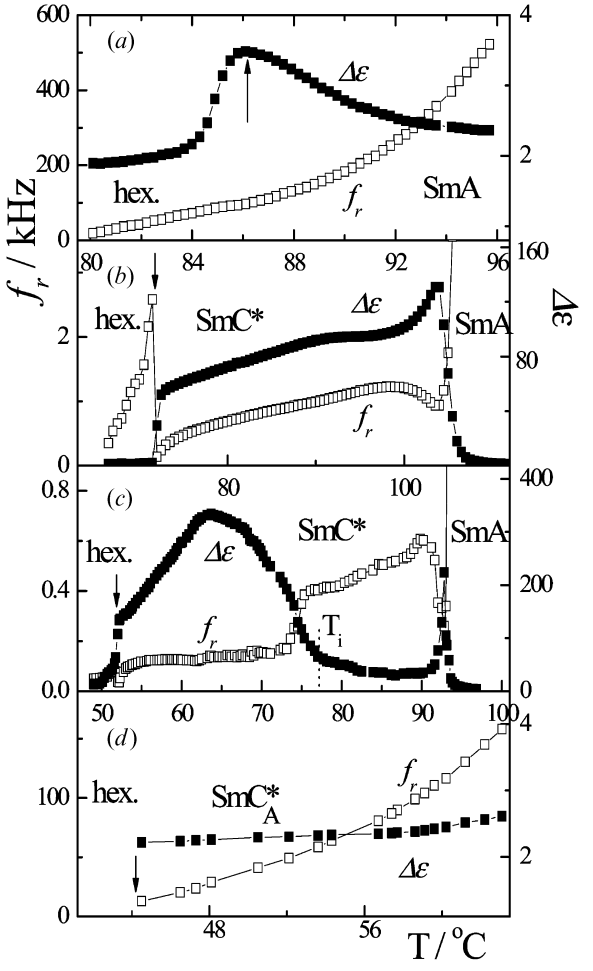


Figure 8. Fitted values of $\Delta\varepsilon$ and $f_r$ for compounds (*a*) **ZLL5/***, (*b*) **ZLLL7/***, (*c*) **ZLL8/6** and (*d*) **ZLL9/***. Arrows designate transition to the hexatic phase. $T_i$ is the temperature of the helix twist inversion.

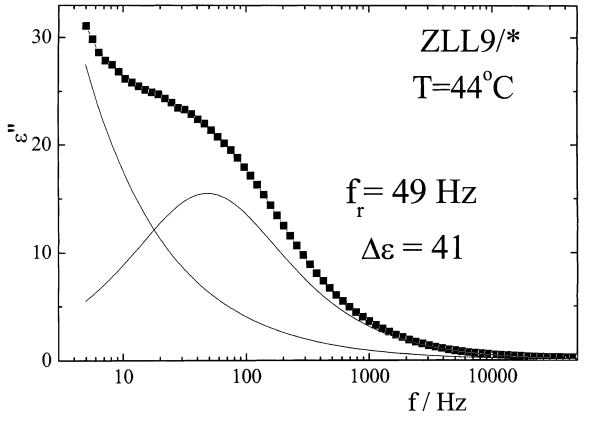


Figure 9. Frequency dependence of the imaginary part of dielectric permittivity for **ZLL9/*** in the SmI*(F*) phase at 44°C. Symbols connected by line show measured values of $\varepsilon''$; full lines present the fitted Cole–Cole plot and low frequency contribution of conductivity.

the Goldstone mode of ideal helicoidal texture can be expressed [13] as:

$$\Delta\varepsilon \cong \frac{1}{K_1}\left(\frac{p\mathbf{P}_S}{\theta_S}\right)^2 \tag{2}$$

where $K_1$ is the twist elastic constant. In real planar samples the structure is a superposition of the helix along the smectic layer normal, parallel to sample surfaces, with the director twist–bend in the perpendicular direction. Theory shows that the dielectric response of such a structure possesses a multirelaxational character, but differs only slightly from the Debye-like dispersion with a relaxation frequency defined as the maximum of losses [14]. When the helix is unwound, the director twist–bend modulation is still present in the planar sample. For the material **ZLL8/6**, below the helix twist inversion temperature, the unwound sample exhibits higher $\Delta\varepsilon$ and lower $f_r$ compared with the helicoidal sample, see figure 8 (*c*). The theory shows that the dielectric response of the real samples is strongly influenced by the internal depolarization field as the rate of change of polarization is so fast that it cannot be compensated completely [14]. The screening of the depolarization field is qualitatively described by a depolarization factor that can be different for each helicoidal and unwound structure. The change of the depolarization factor at the helix unwinding can be considered as the main reason of the jump in $\Delta\varepsilon$ and $f_r$ at the inversion temperature $T_i$.

In the tilted hexatic phase two bond orientation modes (phason and amplitudon) and two tilt angle modes (phason and amplitudon), bilinearly coupled to the polarization, are in principle dielectrically active [4, 12]. The amplitudons are too weak to be observed. Due to the high viscosity of the diffusion of molecular mass centres in the hexatic phase, the hexatic bond-orientation order can be assumed to be frozen. Then the azimuthal molecular tilt fluctuations (Goldstone mode) remain as the strongest mode, which is observed experimentally. The increase of its relaxation frequency and decrease of dielectric strength in the SmI*(F*) phase compared with the SmC* phase can be explained by the appearance of the local hexatic potential, which restricts the azimuthal fluctuations of the molecular tilt [4]. A Goldstone mode with a relatively high dielectric strength and low relaxation frequency is also observed in the hexatic phase below the $SmC^*_A$ phase, confirming the ferroelectric character of this phase.

This work was supported by the Grant Agency of the Czech Republic (Projects No. 202/02/0840 and 202/03/0551), project K1010104 and European Project COST D14 WG 00015.

Downloaded At: 16:48 25 January 2011

## References


[1] KAŠPAR, M., HAMPLOVÁ, V., NOVOTNÁ, V., GLOGAROVÁ, M., POCIECHA, D., and VANĚK, P., 2001, *Liq. Cryst.*, **28,** 1203.

[2] NOVOTNÁ, V., GLOGAROVÁ, M., KAŠPAR, M., and HAMPLOVÁ, V., 2001, *J. chem. Phys.*, **115,** 9036.

[3] PYZUK, W., GÓRECKA, E., SZYDŁOWSKA, J., KROWCZYNSKI, A., and POCIECHA, D., 1995, *Phys. Rev. E*, **52,** 1748.

[4] RYCHETSKÝ, I., GLOGAROVÁ, M., and NOVOTNÁ, V., 2003, *Phys. Rev. E*, **67,** 021 704.

[5] POCIECHA, D., GLOGAROVÁ, M., GORECKA, E., RYCHETSKÝ, I., MIECZKOWSKI, J., and DVORAK, V., 1999, *Mol. Cryst liq. Cryst.*, **328,** 275.

[6] SZYDŁOWSKA, J., POCIECHA, D., GÓRECKA, E., KARDAŚ, D., MIECZKOWSKI, J., and PRZEDMOJSKI, J., 1999, *J. mater. Chem.*, **9,** 361.

[7] KRISHNA PRASAD, S., SHANKAR RAO, D. S., CHANDRASEKHAR, S., NEUBERT, M. E., and GOODBY, J. W., 1995, *Phys. Rev. Lett.*, **74,** 270.

[8] GLOGAROVÁ, M., GÓRECKA, E., LEJČEK, L., and SVERENYÁK, H., 1997, *Mol. Cryst liq. Cryst.*, **301,** 325.

[9] HAMPLOVÁ, V., BUBNOV, A., KAŠPAR, M., NOVOTNÁ, V., LHOTÁKOVÁ, Y., and GLOGAROVÁ, M., 2003, *Liq. Cryst.*, **30,** 1463.

[10] SZYDŁOWSKA, J., POCIECHA, D., MATRASZEK, J., and MIECZKOWSKI, J., 1999, *Liq. Cryst.*, **26,** 1787.

[11] HIRAOKA, K., UEMATSU, Y., TAKEZOE, H., and FUKUDA, A., 1996, *Jpn. J. appl. Phys.*, **35,** 6157.

[12] RYCHETSKÝ, I., GLOGAROVÁ, M., and NOVOTNÁ, V. *Ferroelectrics* (submitted).

[13] BLINC, R., and ŽEKŠ, B., 1978, *Phys. Rev.*, **18,** 740.

[14] RYCHETSKÝ, I., NOVOTNÁ, V., and GLOGAROVÁ, M., 2000, *J. Phys. IV Fr.*, **10,** 119.


Downloaded At: 16:48 25 January 2011